Temperature measurement by visible pyrometry : orthogonal cutting application

Nicolas Ranc, Vincent Pina, Guy Sutter, Sylvain Philippon

Temperature Measurement by Visible Pyrometry: Orthogonal Cutting Application

N. Ranc
e-mail: nicolas.ranc@u-paris10.fr
V. Pina

L.E.E.E., E.A.387, Université de Paris X Nanterre, 1, Chemin Desvallières, 92410 Ville d'Avray, France
Tel.: +33-1-47-09-70-13; Fax: +33-1-47-09-16-45

G. Sutter

S. Philippon

L.P.M.M., U.M.R. C.N.R.S. n°7554, I.S.G.M.P., Université de Metz, Ile du Saulcy, 57045 Metz, France

The working processes of metallic materials at high strain rate like forging, stamping and machining often induce high temperatures that are difficult to quantify precisely. In this work we, developed a high-speed broad band visible pyrometer using an intensified CCD camera (spectral range: 0.4 μm–0.9 μm). The advantage of the visible pyrometry tech-nique is to limit the temperature error due to the uncertainties on the emissivity value and to have a good spatial resolution (3.6 μm) and a large observation area. This pyrometer was validated in the case of high speed machining and more precisely in the orthogonal cutting of a low carbon steel XC18. The cutting speed varies between 22 ms^{-1} and 60 ms^{-1}. The experimental device allows one to visualize the evolution of the temperature field in the chip according to the cutting speed. The maximum temperature in the chip can reach 730°C and minimal temperature which can be detected is around 550°C.

1 Introduction

To understand and model more precisely the transformation processes of metallic materials like forging, stamping and machining, it is necessary to take into account a majority of the various phenomena or parameters occurring during these processes. In most cases, they generate friction and high plastic deformations which dissipate a major part of the mechanical energy into heat.

Temperature is one of the most significant parameters, particularly in high speed processes. One can assume that the thermal phenomena are adiabatic because the heat has not enough time to spread in the material. The temperature rises can be significant and completely modify the manufacturing process. For example the behavior law of materials and the friction coefficient strongly depend on the temperature. To validate the analytical and numerical models, it is necessary to determine the temperature in experiments.

An application, in which the temperature plays an essential role, is machining and more particularly high speed machining [1,2]. Hasting et al. [3] analyze the cutting process from a theory in which the properties of the work piece material depend on the temperature and the strain-rate. Indeed, this manufacturing process generates great strain located mainly in the primary deformation zone and an intense friction on tool-chip interface [4,5]. The temperature in the chip can reach 800–900°C [6]. The optimization of the cutting conditions, as well as the tools damage, depends mainly on the maximum temperature reached. Indeed an increase in the temperature on the tool–chip interface reduces the friction coefficient and thus the cutting pressures, but it affects the tool life [7] and it can also generate a modification of the workpiece material characteristics. The objective of this study is to develop an experimental device to measure the temperature which can be used for transformation processes of metallic materials and validate it for high speed orthogonal cutting. For this purpose, we chose to design and realize a fast pyrometer.

The radiation emitted by the surface of a material depends on its temperature and the wavelength (Planck law [8]) and is also proportional to a factor called emissivity which is a surface characteristic. The dependence of this radiation with the temperature is the principle of pyrometry. Compared with conventional temperature sensors such as thermocouples, this measurement technique has the advantage of being nonintrusive and having a very short response time [9]. It also allows to visualize temperature cartographies. However, the pyrometry presents difficulties related to uncertainty on the surface emissivity. Although measurement techniques eliminating the emissivity have been developed [10,11], they are not easily usable for our study.

The design of a pyrometer consists in choosing a spectral range, which is linked to the measured temperature and the spectral sensitivity of the selected detector. If the spectral bandwidth is reduced to a few tens of nanometers (limited by an interference filter for instance) we consider that the pyrometry is monochromatic [6]. On the contrary if the bandwidth is broad, we will use the polychromatic pyrometry technique [12].

The spectral band associated with the thermal radiation is commonly limited to wavelengths ranging between 0.1 μm and 100 μm. In this range, the behavior of electromagnetic waves strongly depends on their wavelength. This spectral band is divided into several regions: ultraviolet ray, visible, near infrared, mid-infrared, and far infrared (Fig. 1). By taking account of the atmosphere absorption, the visible and near infrared fields are cutting out in three observation spectral bands (band I: 0.5–2 μm; band II: 3–5 μm; band III: 8–12 μm). Detectors are used to measure the power radiated by a surface. Their operation principle can be very different but we can distinguish two principal families: thermal detectors and quantum detectors.

1.1 Thermal Detectors. In the case of the thermal detectors, incident radiation causes an increase in temperature of the detector surface. The measurement of this temperature variation allows one to quantify the received energy. This type of detector has a constant spectral sensitivity in relatively broad spectral bands. However its principal drawback is the relatively long response time (approximately 10^{-3} s).

1.2 Quantum Detectors. The quantum detectors are made of materials which absorb incident radiation by producing free or semi free charge carriers (photovoltaic or photoconductor detector) or by ejecting an electron by photo emission (photoemissive detector). The principal semiconductors used in the photovoltaic and photoconductive detectors are silicon (Si), germanium (Ge), the indium antimonide (InSb) and the mercury cadmium telluride (HgCdTe also noted MCT) (Table I). The photovoltaic detectors are generally more sensitive and faster than the photoconductors. To obtain a better detectivity, these detectors are often cooled at the liquid nitrogen temperature (77 K).

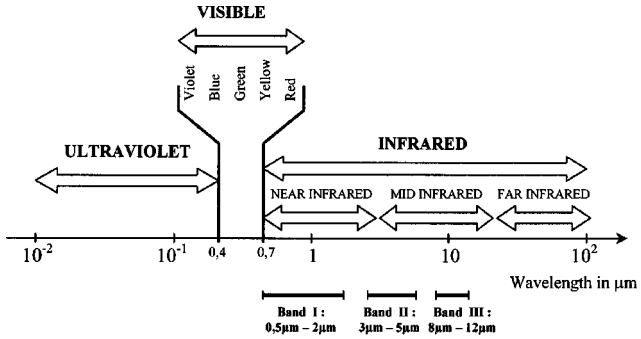

Fig. 1 Thermal radiation spectrum

The photoemissive detectors are composed of a photocathode placed in a vacuum. When this photocathode is struck by an incident photon it causes the expulsion of an electron in vacuum. The released electron is then accelerated towards the anode and contributes to create a current. This type of detector is rather sensitive to short wavelengths (ultraviolet, visible, and near infrared), because the energy of the incident photon must be sufficient to eject the electron. The materials used to carry out the photocathode and their spectral sensitivity are given in Table I. In a photomultiplier, the signal can also be amplified by a succession of dynodes (polarized electrodes) allowing starting from an emitted electron, to release several from them. On the same principle, an intensified charge-coupled-device (CCD) camera consists of a slightly glass substrate with millions of parallel traversing channels of few ten micrometers of diameter containing a secondary electron emitter. Electrons generated by the photocathode are driven through the channels by a constant field from a high voltage applied to the microchannel plate. An electron passing through strikes the walls, causing the formation of more electrons. A single entering electron can produce several thousands of electrons that finally exit from the plate.

Pyrometry techniques are often used for the study of the dynamic behavior of materials: Ravichandran et al. use a matrix of 8×8 HgCdTe Infrared detectors [13] to measure the field of temperature in an adiabatic shear band (between 30°C and 100°C) [14] or at the head of the crack [15]. The spatial resolution of their device is about one hundred micrometers with a response time of about a microsecond. In a previous study, we measured the maximum temperature reached in adiabatic shear bands in the visible range using a monochromatic pyrometer at 0.634 μm [16]. With this technique, it is possible to obtain only one thermography with an aperture time of 6 μs and a spatial resolution of 5 μm.

Many authors were interested in the temperature measurements during high speed machining [6]. More recently we have determined the temperature field in the cutting zone during an orthogonal high speed machining operation of 42CD4 steel [6]. We used a monochromatic pyrometer with an interference filter at 0.8 μm to study the influence of the cutting speed and the chip thickness on the temperature profile.

In this article, we develop a broad band visible pyrometer particularly adapted with high speed machining of low carbon steel XC18. This steel forms a continuous chip and the temperature is about 500°C (lower than for the 42CD4 steel). A broad band pyrometer allows one to detect lower temperature than a monochromatic pyrometer. After some remarks on the solid radiation in Sec. 2, we will justify our choices in the design of the broadband pyrometer. The thermographies obtained in this work and in particular the influence of the cutting speed on the temperature field are presented in Sec. 4. The measurement errors due to emissivity values are also discussed.

Table 1 Principal photosensitive materials

Photosensitive material	Range of sensibility	Sensor type
Si	0.4 μm–1.1 μm	Photovoltaic
InSb	1 μm–5.5 μm	Photovoltaic
HgCdTe	2 μm–14 μm	Photovoltaic Photoconductor
PbS	1.3 μm–3 μm	Photoconductor
Bialkali coating (Sb–Rb–Cs;Sb–K–Cs)	0.15 μm–0.65 μm	Photoemissive
Multialkali coating S_{20} (Na–K–Sb–Cs)	0.15 μm–0.85 μm	Photoemissive
AsGa (GEN III)	0.3 μm–0.9 μm	Photoemissive

2 Pyrometry Technique

2.1 Radiation of Solids. The intensity is the power radiated in a direction $\boldsymbol{\delta}$ by a unit surface in a solid angle of one steradian. The radiation dP emitted by a surface dS with a normal $\mathbf{n}$ in a solid angle $d\Omega$ of direction $\boldsymbol{\delta}$ is related to the intensity I:

$$dP = I(\boldsymbol{\delta})\,\boldsymbol{\delta}\cdot\mathbf{n}\,d\Omega\,dS \tag{1}$$

The intensity depends on the radiation wavelength. We can also define the spectral intensity noted I_λ by the following relation:

$$I_\lambda = \frac{\partial I}{\partial \lambda} \tag{2}$$

A blackbody absorbs completely any incident radiation, whatever its wavelength. The spectral intensity of a blackbody noted I^0_λ at the temperature T is given by Planck's law [17]:

$$I^0_\lambda(\lambda,T) = \frac{C_1\lambda^{-5}}{\exp\left(\dfrac{C_2}{\lambda T}\right)-1} \tag{3}$$

With $C_1 = 2hc^2$ and $C_2 = hc/k$ the first and second radiation constants, $k = 1.380\,662.10^{-23}\,\mathrm{J\,K^{-1}}$ the Boltzman constant, $h = 6.626\,176.10^{-34}\,\mathrm{J\,s}$ the Planck constant and $c = 2.998.10^{8}\,\mathrm{ms^{-1}}$ the light celerity in vacuum.

Generally for the short wavelengths ($\lambda T \ll C_2 = 14{,}388\,\mu\mathrm{m\,K}$), we use the Wien approximation:

$$\exp\left(\frac{C_2}{\lambda T}\right) \gg 1 \tag{4}$$

With this approximation, the Planck law becomes then

$$I^0_\lambda(\lambda,T) = \frac{C_1\lambda^{-5}}{\exp\left(\dfrac{C_2}{\lambda T}\right)} \tag{5}$$

For a given temperature, the spectral intensity of the blackbody shows a maximum for a wavelength λ_{max} (Fig. 2). This wavelength is given by the Wien law:

$$\lambda_{max} = \frac{C_2}{5}\,\frac{1}{T} \tag{6}$$

For a temperature of 700°C this maximum is in the near infrared band at a wavelength of 2.96 μm. When the temperature decreases this maximum of intensity is shifted towards the big wavelengths (infrared range).

Another significant quantity is the radiance sensitivity to the temperature variations. This sensitivity is characterized by the ratio $(1/I^0_\lambda)(\partial I^0_\lambda/\partial T)$. For a blackbody we have:

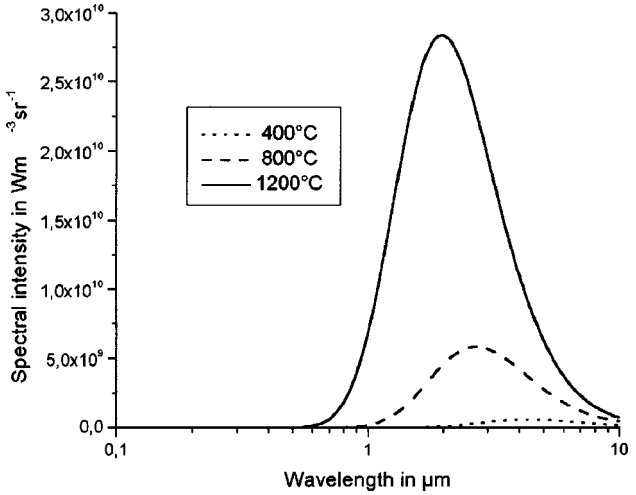

Fig. 2 Blackbody spectral intensity for the temperatures of 400°C, 800°C, and 1200°C

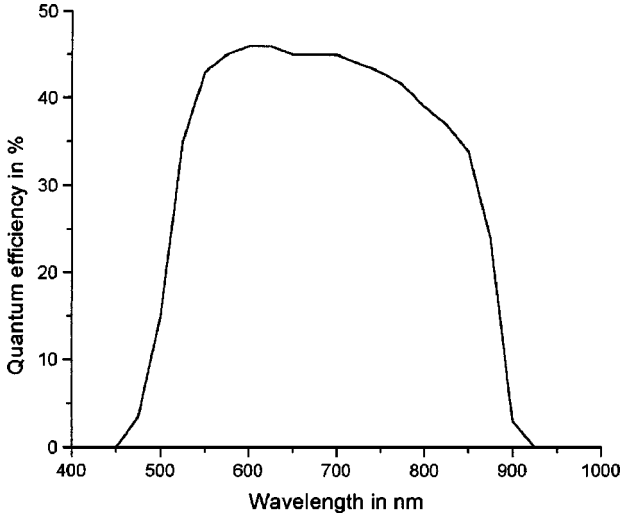

Fig. 4 Quantum efficiency of the intensified camera

$$\frac{1}{I_\lambda^0}\frac{\partial I_\lambda^0}{\partial T}=\frac{C_2}{\lambda T^2}\frac{\exp\left(\frac{C_2}{\lambda T}\right)}{\exp\left(\frac{C_2}{\lambda T}\right)-1} \tag{7}$$

This sensitivity is represented in Fig. 3 for the temperatures of 400°C, 800°C, and 1200°C according to the wavelength. We can observe that this sensitivity becomes very high for the short wavelengths (ultraviolet field).

The behavior of a real surface is different from a blackbody's. We can express its intensity as

$$I_\lambda(\lambda,T)=\varepsilon_\lambda(\lambda,T)I_\lambda^0(\lambda,T)$$

$$\text{with } \varepsilon_\lambda(\lambda,T) \text{ the spectral emissivity} \tag{8}$$

The emissivity characterizes the radiation of a real surface compared to the radiation of a blackbody at the same temperature and placed under the same conditions. This factor always lies between 0 and 1 (the case $\varepsilon=1$ corresponds to the blackbody). Moreover, the surface emissivity depends on the material [18–22]; the surface roughness [21–23]; the physical state of material (solid or liquid) [19,21,24]; the surface temperature [19–21]; the direction for emission [22,23,25]; the wavelength [18,20,21].

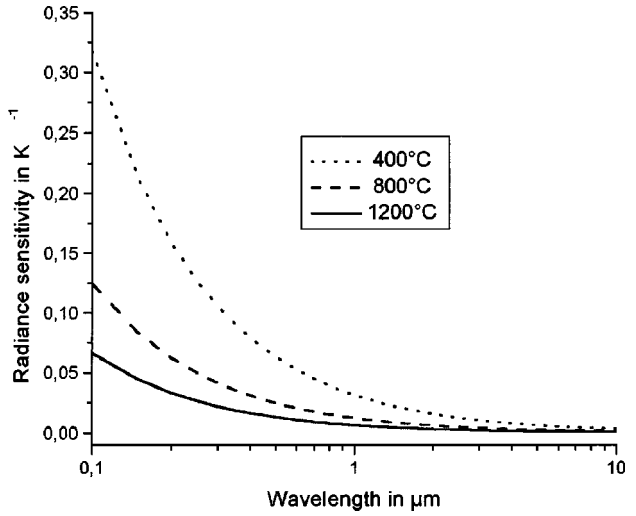

Fig. 3 Radiance sensitivity to the temperature variations for the temperatures of 400°C, 800°C, and 1200°C

2.2 Principle of Pyrometry. The measurement technique by pyrometry is achieved through measuring the power radiated by a surface using a detector in order to deduce its temperature. If we make the assumption that the surface behaves like a blackbody, we can determine a radiance temperature (T_λ) also called the blackbody equivalent temperature. This radiance temperature is always lower or equal to the real temperature of the surface. If we need to know the real temperature, it is necessary to determine the surface emissivity.

In this article, we try to minimize the difference between the real temperature and radiance temperature. Indeed, Fig. 3 shows that the shorter the wavelength is, the higher the sensitivity to variations in temperature is, and the weaker the error between the real temperature and the radiance temperature will be. The advantage of this technique is that the dependence of temperature on emissivity is greatly reduced.

3 Experimental Device

3.1 Choice of the Detector and the Optical Device. The choice of the wavelength of the pyrometer is a compromise between a maximum sensitivity and a sufficient level of radiated power which can be detected. For this study, we chose an intensified camera whose spectral band is located in the visible (0.4 μm to 0.9 μm). Figure 4 represents the quantum efficiency $\eta(\lambda)$ of the camera according to the wavelength which is given by the manufacturer. In order to collect the maximum of the radiated power, the entire spectral band of the camera was used. The aperture time can vary between 5 ns and a few milliseconds. We carried out only one image during an orthogonal cutting test because the refresh time of the CCD is much larger than the machining duration.

To focus the maximum of energy, we use an objective with a 50 mm focal length. This optical device enables one to obtain a very good resolution: a pixel corresponds to approximately 3.6 μm and the surface observed is a square of 3.7×3.7 mm.

3.2 Temperature Determination: Calibration Curves The pyrometer is calibrated on a blackbody for temperatures between 500°C and 900°C. Three aperture times of 150 μs, 200 μs, and 600 μs were selected. They correspond to the durations of complete machining of the specimen for speeds of 60 ms^{-1}, 38 ms^{-1}, and 22 ms^{-1}. Figure 5(a) represents the measured level of a pixel Si for different blackbody temperatures and for each aperture time. The blackbody temperature varies between 500°C and

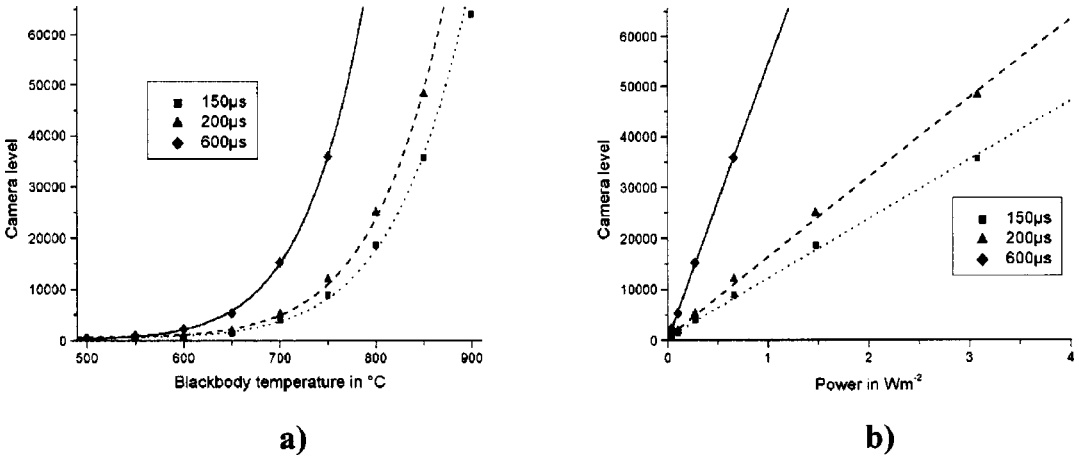

Fig. 5 Calibration curves. (a) Representation according to the temperature. (b) Representation according to the power

900°C with an increment of 50°C. In Fig. 5(b), we draw the level of pixel versus the power received by the detector $E(T)$:

$$E(T)=\int_0^\infty \eta(\lambda) I_\lambda^0(\lambda,T)\,d\lambda \tag{9}$$

We can consider that the relation between Si and $E(T)$ is linear. Then we have:

$$\mathrm{Si}=\mathrm{Si}^0+k\cdot E(T) \tag{10}$$

Si^0 and k are two calibration constants, which depend on the camera, the optical device and the acquisition chain. To identify them simply, we represent the evolution of Si according to $E(T)$ and we determine the parameters Si^0 and k by a linear regression. Also, the evolution of the pixel level is also traced according to the temperature for each aperture time in Fig. 5(a).

3.3 A Technical Application: A High Speed Machining. To validate the pyrometer presented above, we performed an application to the measurement of the temperature field during a high speed machining process. The mechanical device of machining was developed by Sutter et al. [26], to investigate high cutting speed allowing to reach 100 m/s and perfectly reproduces orthogonal cutting conditions. This device reduces the problems observed in the conventional machine tools (for example the maximum cutting speed, parasite vibrations). Dry cutting conditions are chosen according to the future orientation in machining. The great accessibility for photographic recordings allows an easy adaptation of the device for optical temperature measurement. Vernaza-Pena et al. [27] also observed experimentally the temperature distribution during orthogonal cutting of an aluminum alloy with HgCdTe infrared detectors.

The parallelepipedal specimen is placed on a projectile and is cut out by two fixed tools (Fig. 6). The two tools are symmetrically positioned to balance the force during machining and to ensure a constant depth of cut. The projectile is animated with a translatory motion in the launch tube by the relaxation of compressed air. The launch tube ensures a precise guiding of the projectile and the specimen. At the end of the launch tube, the specimen is machined by the tools. A second tube, called a receiving tube, supports the tools and drives the projectile towards a shock absorber after machining.

A wide range of cutting speed is possible with this device (from 10 to 100 ms^{-1}). The speed is measured by photodiodes and a time counter. All tests are carried out using carbide tools without a chip-breaker. The rake angle, α, can vary with slope of the tool but all the tests presented here were made with α=0 deg. To neglect the wear effects, the tools are changed for each shot. Before and after each test, the length of the specimen is measured to determine the chip thickness t_1. This value is confirmed by the photographic recordings which allow a measurement of t_1 during the chip formation [Figs. 7(a) and 7(b)].

4 Results and Discussion

4.1 Presentation of Thermographies. The aperture time of the camera is slightly lower than the duration of specimen machining. The difference between the aperture time and the machining duration are 146 μs, 63 μs, and 16 μs, respectively for the speed of 22 ms^{-1}, 38 ms^{-1}, and 60 ms^{-1}. During this aperture time, the temperature field in chip is supposed to be stationary. After analysis of the images recorded for the different cutting speeds and also taking into account the corresponding calibration curves, we obtain the thermographies presented in Fig. 8. The effect of the cutting speed on the maximum temperature level in the chip can also be studied. We observe an increase in the maximum of temperature with the cutting speed. This increase in temperature is more significant for low speed than for high speeds. Between 22 ms^{-1} and 38 ms^{-1}, there is an increment of 80°C, whereas between 38 ms^{-1} and 60 ms^{-1} we have an increment of only 15°C. A similar tendency was already observed for another steel [6] and other cutting conditions like oblique turning process with a localized temperature measurement at the tool–chip interface [28].

One of the advantages of this device is to record the chip formation without changing the camera and the visualization zone. The chip is enlightened with a flash and the camera is opened

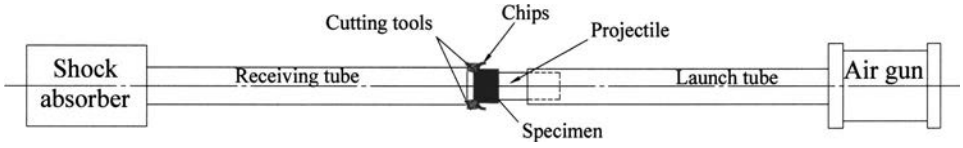

Fig. 6 Mechanical device of orthogonal cutting

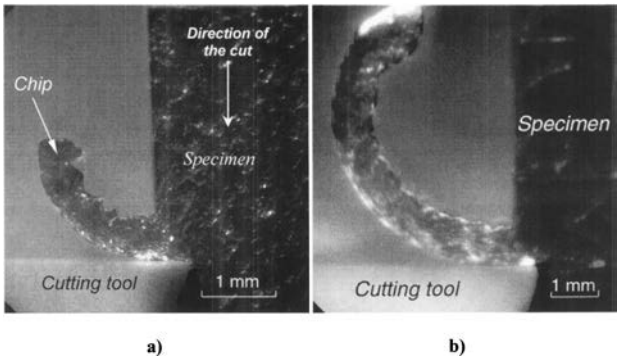

Fig. 7 Photographic recording of chip formation during the process of orthogonal cutting. (a) $t_1 = 0.49$ mm, $V_c = 17$ ms^{-1}, $\alpha = 0$ deg; (b) $t_1 = 0.54$ mm, $V_c = 60$ ms^{-1}, $\alpha = 0$ deg

during approximately one microsecond. We performed the images presented in Figs. 7(a) and 7(b). We can notice that the chip remains continuous and does not segment. We showed that the field of temperature in the zone of machining can be regarded as stationary during machining [6]. Therefore we can consider that the temperature in the chip remains constant during the aperture time.

4.2 Error Measurement on *T*. As we said previously, the approximation between the real temperature and the radiance temperature introduces errors related to the emissivity. During machining, this factor varies because it depends on the temperature and the roughness of the surface of specimen. During the plastic deformation, there is an increase in the surface roughness and therefore in the emissivity.

At first, to estimate these errors, we make the assumption that for the weak variations of roughness and measured temperature (between 600°C and 700°C), the emissivity varies little. We can determine the surface radiance temperature T_λ with the relation (10) according to the signal Si:

$$T_\lambda = E^{-1}\left(\frac{\mathrm{Si} - \mathrm{Si}^0}{k}\right) \tag{11}$$

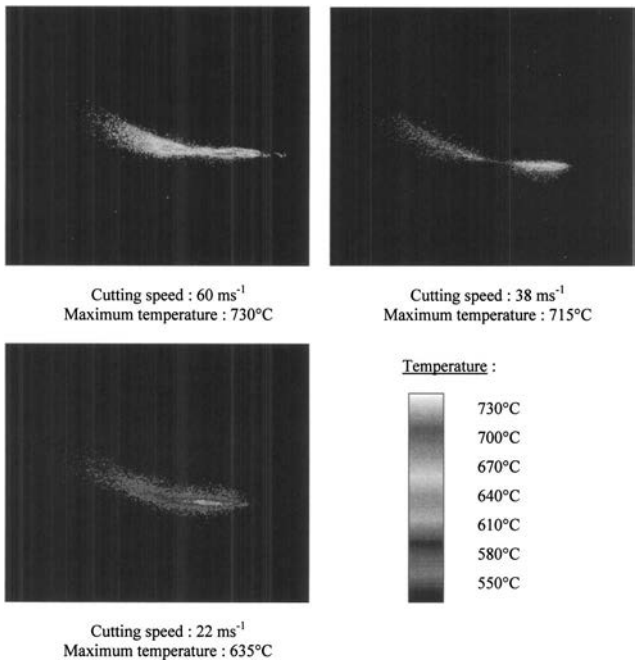

Fig. 8 Chip thermography for different cutting speeds

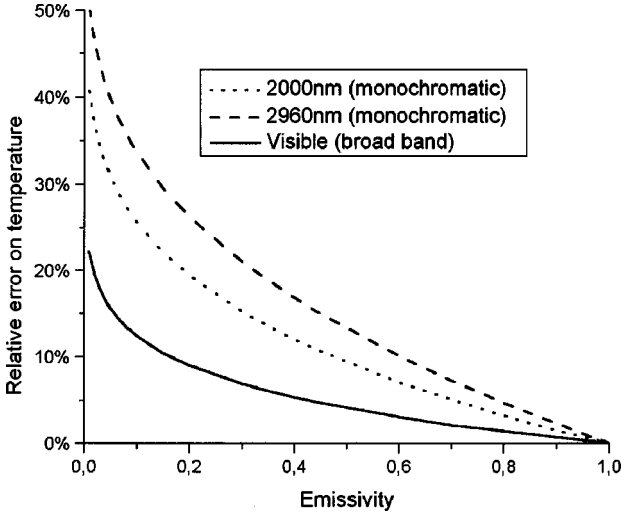

Fig. 9 Error on the temperature measurement according to the emissivity at a temperature of 800°C

The inverse function E^{-1} will be calculated numerically.

The real surface temperature can be expressed according to the detector signal and the emissivity:

$$\mathrm{Si} = \mathrm{Si}^0 + k \cdot E'(T) \quad \text{with} \quad E'(T) = \int_0^\infty \eta(\lambda)\varepsilon_\lambda(\lambda, T) I_\lambda^0(\lambda, T)\, d\lambda \tag{12}$$

If we consider that the emissivity is constant in the spectral band of the camera (0.4 μm–0.9 μm), we obtain

$$\mathrm{Si} = \mathrm{Si}^0 + k\varepsilon_\lambda \cdot E(T) \tag{13}$$

We can express the error as:

$$\Delta T = T - T_\lambda = E^{-1}\left(\frac{\mathrm{Si} - \mathrm{Si}^0}{k\varepsilon_\lambda}\right) - E^{-1}\left(\frac{\mathrm{Si} - \mathrm{Si}^0}{k}\right) \tag{14}$$

The quantification of the error consists of estimating the value of the emissivity, either using bibliographical data [29], or by a direct measurement during a static test in a vacuum chamber. The knowledge of the emissivity values allows us to limit its evolution range.

The relative error between the real temperature and the radiance temperature is represented in Fig. 9 versus emissivity at a temperature of 800°C for infrared and visible domains. In the visible spectral band, the order of magnitude of emissivity is 0.4 [29]. It increases with the roughness and the temperature. The maximum relative error is then 5.3%. A variation of 10% of the emissivity causes a relative error of 0.5% on temperature.

In the case of monochromatic infrared pyrometry at 2.96 μm wavelength and with a band width of 10 nm, the order of magnitude of emissivity is generally lower than in the visible and the uncertainty on the temperature is around 21% for an emissivity of 0.3. A variation of 10% of the emissivity causes a relative error of 1.3% on temperature. These error values are indeed higher in infrared than in the visible. The relative error on temperature is represented in Fig. 10 versus temperature for an emissivity value of 0.4 in the visible domain (0.4 μm–0.8 μm) and 0.3 in the infrared domain (2.96 μm–2.00 μm).

5 Conclusion

The working processes of metallic materials at high strain rate often induce high temperatures that it is necessary to quantify precisely. The knowledge of these temperatures is an invaluable help to understand the mechanisms which take place during the industrial process. In this article, we developed a high-speed

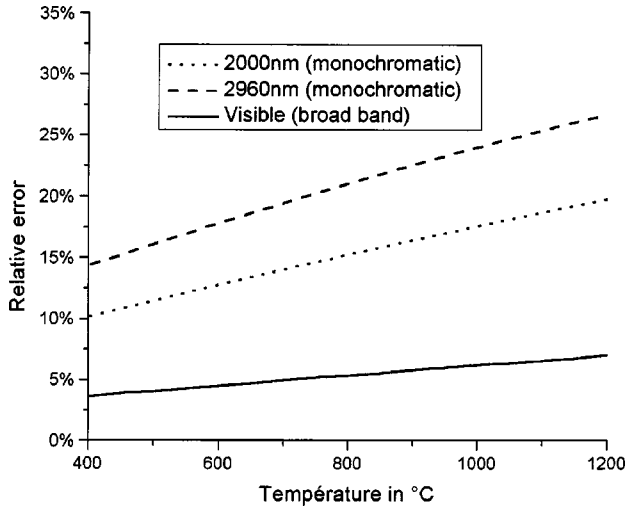

Fig. 10 Error on the temperature measurement according to the temperature for a fixed emissivity

broad band pyrometer. Its visible spectral range is particularly adapted to the temperature range of this type of process. The spectral band between 0.4 μm and 0.9 μm was chosen in order to obtain a maximum sensitivity and a sufficient radiated power which can be detected. The choice of a maximum sensitivity and thus a smallest possible wavelength allows one to limit the error due to the emissivity.

Another advantage of the visible pyrometer is to have a good spatial resolution (3.6 μm). The broad band pyrometry allows one to measure lower temperature than monochromatic pyrometry at 0.8 μm wavelength and to keep the same sensitivity. In Fig. 10 the temperature errors for broad band and monochromatic pyrometry are equal.

This pyrometer was validated in the case of high speed machining and more precisely in orthogonal cutting. This experimental device allows one to visualize the evolution of the temperature field in the chip according to the cutting speed.

References

[1] Milton, C., and Shaw, M. C., 1984, *Metal Cutting Principles*, Clarendon Press, Oxford Science Publication, UK.

[2] Loewen, E. G., and Shaw, M. C., 2000, ''On the Analysis of Cutting Tool Temperature,'' Trans. Am. Soc. Mech. Engrs., **71**, pp. 217–231.

[3] Hastings, W. F., Mathews, P., and Oxley, P. L. B., 1980, ''A Machining Theory for Predicting Chip Geometry, Cutting Forces Etc. From Material Properties and Cutting Conditions,'' Proc. R. Soc. London, Ser. A, **371**, pp. 569–587.

[4] Doyle, E. D., Homme, J. G., and Tabor, D., 1979, ''Frictional Interaction Between Chip and Rake Face in Continuous Chip Formation,'' Proc. R. Soc. London, Ser. A, **3666**, pp. 176–183.

[5] Grzesik, W., 2003, ''Friction Behavior of Heat Isolating Coating in Machining: Mechanical, Thermal and Energy-Based Considerations,'' Int. J. Mach. Tools Manuf., **43**, pp. 145–150.

[6] Sutter, G., Faure, L., Molinari, A., Ranc, N., and Pina, V., 2003, ''An Experimental Technique for the Measurement of Temperature Fields for the Orthogonal Cutting in High Speed Machining,'' Int. J. Mach. Tools Manuf., **43**, pp. 671–678.

[7] Ay, H., and Yang, W. J., 1998, ''Heat Transfer and Life of Metal Cutting Tools in Turning,'' Int. J. Heat Mass Transfer, **43**, pp. 613–623.

[8] Planck, M., 1901, ''Distribution of Energy,'' Ann. Phys. (N.Y.), **4**, 3, pp. 553–563.

[9] Childs, P. R. N., Greenwood, J. R., and Long, C. A., 2000, ''Review of Temperature Measurement,'' Rev. Sci. Instrum., **71**, 8, pp. 2959–2978.

[10] Murray, T. P., 1967, ''Polaradiometer: A New Instrument for Temperature Measurement,'' Rev. Sci. Instrum., **38**, pp. 791–798.

[11] Hervé, P., 1983, ''Mesure simultanée de la température de surface et de son émissivité,'' Measurement, **485**, pp. 20–24.

[12] Duvaut, T., Georgeault, D., and Beaudoin, J. L., 1995, ''Multiwavelength Infrared Pyrometry: Optimization and Computer Simulations,'' Infrared Phys. Technol., **36**, pp. 1089–1103.

[13] Zehnder, A. T., Guduru, P. R., Rosakis, A. J., and Ravichandran, G., 2000, ''Million Frames Per Second Infrared Imaging System,'' Rev. Sci. Instrum., **71**, 10, pp. 3762–3768.

[14] Guduru, P. R., Ravichandran, G., and Rosakis, A. J., 2001, ''Observation of Transient High Vortical Microstructures in Solids During Adiabatic Shear Banding,'' Phys. Rev. E, **64**, pp. 1–6.

[15] Guduru, P. R., Zehnder, A. T., Rosakis, A. J., and Ravichandran, G., 2001, ''Dynamic Full Field Measurements of Crack Tip Temperatures,'' Eng. Fract. Mech., **68**, pp. 1535–1556.

[16] Ranc, N., Pina, V., and Hervé, P., 2000, ''Optical Measurements of Phase Transition and Temperature in Adiabatic Shear Bands in Titanium Alloys,'' J. Phys. IV, **10**, pp. 347–352.

[17] Modest, M. F., 1993, *Radiative Heat Transfert*, McGraw–Hill, New York.

[18] Palik, E. D., 1985, *Handbook of Optical Constants*, Academic, New York.

[19] Piriou, B., 1973, ''Mise au point sur les facteurs d'émission,'' Rev. Int. Hautes Temp. Refract., **10**, pp. 283–295.

[20] Hampartsoumian, E., Hainsworth, D., Taylor, J. M., and Williams, A., 2001, ''The Radiant Emissivity of Some Materials at High Temperatures-Review,'' J. Inst. Energy, **74**, pp. 91–99.

[21] Hiernaut, J. P., Beukers, R., Hoch, M., Matsui, T., and Ohse, R. W., 1986, ''Determination of the Melting Point and of the Spectral and Total Emissivities of Tungsten, Tantalum and Molybdenum in the Solid and Liquid States With a Six-Wavelength,'' High Temp. - High Press., **18**, pp. 627–633.

[22] Dunkle, R. V., 1960, ''Thermal Radiation Characteristics of Surfaces,'' Theory and fundamental research in heat transfer: Proceedings of the Annual Meeting of the American Society of Mechanical Engineers, New York.

[23] Hervé, P., 1977, ''Influence de l'état de surface sur le rayonnement thermique des matériaux solides,'' Ph.D. thesis, Paris VI.

[24] Antoni Zdziobek, A., Pina, V., Hervé, P., and Durand, F., 1997, ''A Radiative Thermal Analysis Method for Phase Change Determination of Strictly Controlled Refractory Alloys,'' High Temp. Mater. Sci., **37**, pp. 97–114.

[25] Birkebak, R. C., and Eckert, E. R. G., 1965, ''Effects of Roughness of Metal Surfaces on Angular Distribution of Monochromatic Reflected Radiation,'' ASME J. Heat Transfer, **87**, pp. 85–94.

[26] Sutter, G., Molinari, A., Faure, L., Klepaczko, J. R., and Dudzinski, D., 1998, ''An Experimental Study of High Speed Orthogonal Cutting,'' ASME J. Manuf. Sci. Eng., **12**, pp. 169–172.

[27] Vernaza-Pena, K. M., Mason, J. J., and Li, M., 2001, ''Experimental Study of the Temperature Field Generated During Orthogonal Machining of an Aluminum Alloy,'' Exp. Mech., **42**, 2, pp. 221–229.

[28] Muller, B., 2001, ''Temperature Measurements With a Fibre-Optic Two-Color Pyrometer,'' Scientific Fundamentals of High Speed Cutting, edited by H. Schulz, Carl Hanser Verlag, München-Wien, pp. 181–186.

[29] Touloukian, Y. S., and DeWitt, D. P., 1970, *Thermophysical Properties of Matter—Thermal Radiative Properties*, IFI/Plenum, New York, Washington, Vol. 7.